Biomass chitosan-derived nitrogen-doped carbon modified with iron oxide for the catalytic ammoxidation of aromatic aldehydes to aromatic nitriles

Wei David Wang [a],*, Fushan Wang [b], Youcai Chang [c], Zhengping Dong [a],*

[a] State Key Laboratory of Applied Organic Chemistry, College of Chemistry and Chemical Engineering, Lanzhou University, Lanzhou, Gansu 730000, PR China
[b] Lanzhou Petrochemical Company, PetroChina, Lanzhou 730060, PR China
[c] Gansu Yinguang Juyin Chemical Co., Ltd, Baiyin, Gansu 730900, PR China

ARTICLE INFO

ABSTRACT

Nitrogen-doped carbon catalysts have attracted increasing research attention due to several advantages for catalytic application. Herein, cost-effective, renewable biomass chitosan was used to prepare a N-doped carbon modified with iron oxide catalyst (Fe_2O_3@NC) for nitrile synthesis. The iron oxide nanoparticles were uniformly wrapped in the N-doped carbon matrix to prevent their aggregation and leaching. Fe_2O_3@NC-800, which was subjected to carbonization at 800 °C, exhibited excellent activity, selectivity, and stability in the catalytic ammoxidation of aromatic aldehydes to aromatic nitriles. This study may provide a new method for the fabrication of an efficient and cost-effective catalyst system for synthesizing nitriles.

1. Introduction

Doping with nitrogen atoms can regulate the electron density of carbon materials, thereby considerably improving the conductivity, surface activity, and surface hydrophilicity of N-doped carbon (NC) materials [1,2]. In addition, it also contributes to the excellent performance of N-doped carbon catalysts in various catalytic reactions [3–5]. Recent studies have reported that N-doped nanostructured carbon derived from renewable biomaterials exhibits high activity [6–8]. Notably, as one of the renewable bioresources, chitosan is not only cost-effective but also abundant, and it can be produced by the deacetylation of chitin, which widely exists in the shell or exoskeleton of shrimps, crabs, and other arthropods in nature. Renewable chitosan is a more cost-effective precursor for the preparation of N-doped carbon materials compared with that of other carbon materials such as nanotubes and graphene [9–11].

Conventional nitrile synthesis methods require highly poisonous metal cyanides as precursors and an additional carbon atom from the cyanide nucleophile at high temperature. In addition, nitriles can be obtained from corresponding substrates containing amines [12], amides [13], alcohols [14], and aldoximes [15] by the dehydration of oxime intermediates or the oxidation of imine intermediates. However, these methods often require high temperature and strong oxidants. An attractive alternative pathway is the direct oxidative synthesis of nitriles

from aldehydes using hexamethyldisilazane, NaN_3, and $K_3[Fe(CN)_6]$ as the nitrogen source or using I_2, sulfuryl fluoride, and $TiCl_4$ as the catalysts under mild reaction conditions [16–20]. However, the above-mentioned methods are toxic or produce considerable amounts of by-products. And a majority of these methods exhibit some disadvantages, such as poor selectivity or narrow range of synthetic substrates for producing diverse nitriles. Hence, it is crucial to develop an environmentally friendly and efficient strategy to produce nitriles.

Heterogeneous catalysts with transition-metal@N-doped carbons exhibit excellent properties for the further improvement of their activity and stability, and the metal particles wrapped within often exhibit superior synergistic effects [21–25]. Remarkably, iron-based N-doped carbons have been widely investigated because the transition-metal iron is abundant, and it exhibits low toxicity and a low price [26–28]. Hence, iron-based N-doped carbons can be a suitable candidate for replacing some current precious-metal-based catalysts. Due to these advantages, in-depth studies have been performed to improve the activity of iron@N-doped carbons and realize environmentally benign syntheses in recent years [29–31]. Clearly, iron oxide exhibits exquisite selectivity for nitriles, which is the precursor for advanced chemicals, bioactive molecules, and natural materials [32].

In this study, Fe_2O_3@NC catalysts were successfully synthesized using renewable biomass chitosan, cost-effective urea, and abundant ferric chloride as starting materials (Scheme 1). Fe_2O_3 nanoparticles
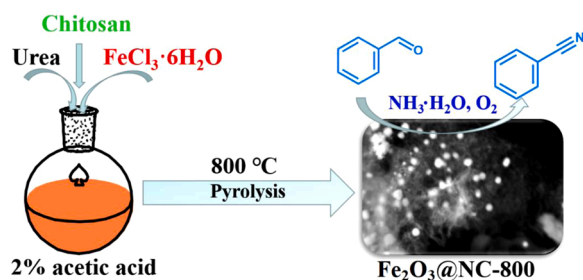
Scheme 1. The preparation procedure and catalytic ammoxidation application of Fe$_2$O$_3$@NC-800 catalyst.

(NPs) were wrapped within chitosan-derived N-doped carbons, which enhanced the stability of Fe$_2$O$_3$ in catalysis. Notably, Fe$_2$O$_3$@NC-800 (Fe$_2$O$_3$@NC catalyst calcinated at 800 °C) exhibited excellent catalytic activity, selectivity, and stability for nitrile synthesis from the ammoxidation of benzaldehydes. In this heterogeneous catalysis, using

ammonia as a green nitrogen source for the ammoxidation reaction represents the green synthesis advantage. Thus, this study may open a cost-effective and environmentally friendly strategy for aromatic nitrile synthesis.

2. Results and discussion

2.1. Catalyst preparation and characterization

The processes of the catalyst preparation and the catalytic ammoxidation of benzaldehydes to benzonitriles are shown in Scheme 1. The detailed synthesis procedures are provided in the Supporting Information. And the successful preparation of Fe$_2$O$_3$@NC catalysts is further investigated as following.

TGA analysis of the as-made Fe$_2$O$_3$@NC catalyst precursor shows the evolution of precursor material through heating (Fig. S1). Marginal weight loss at temperatures of less than 144 °C was observed for the precursor material probably due to water loss. With increase in calcination temperature, the urea in the precursor started to decompose.
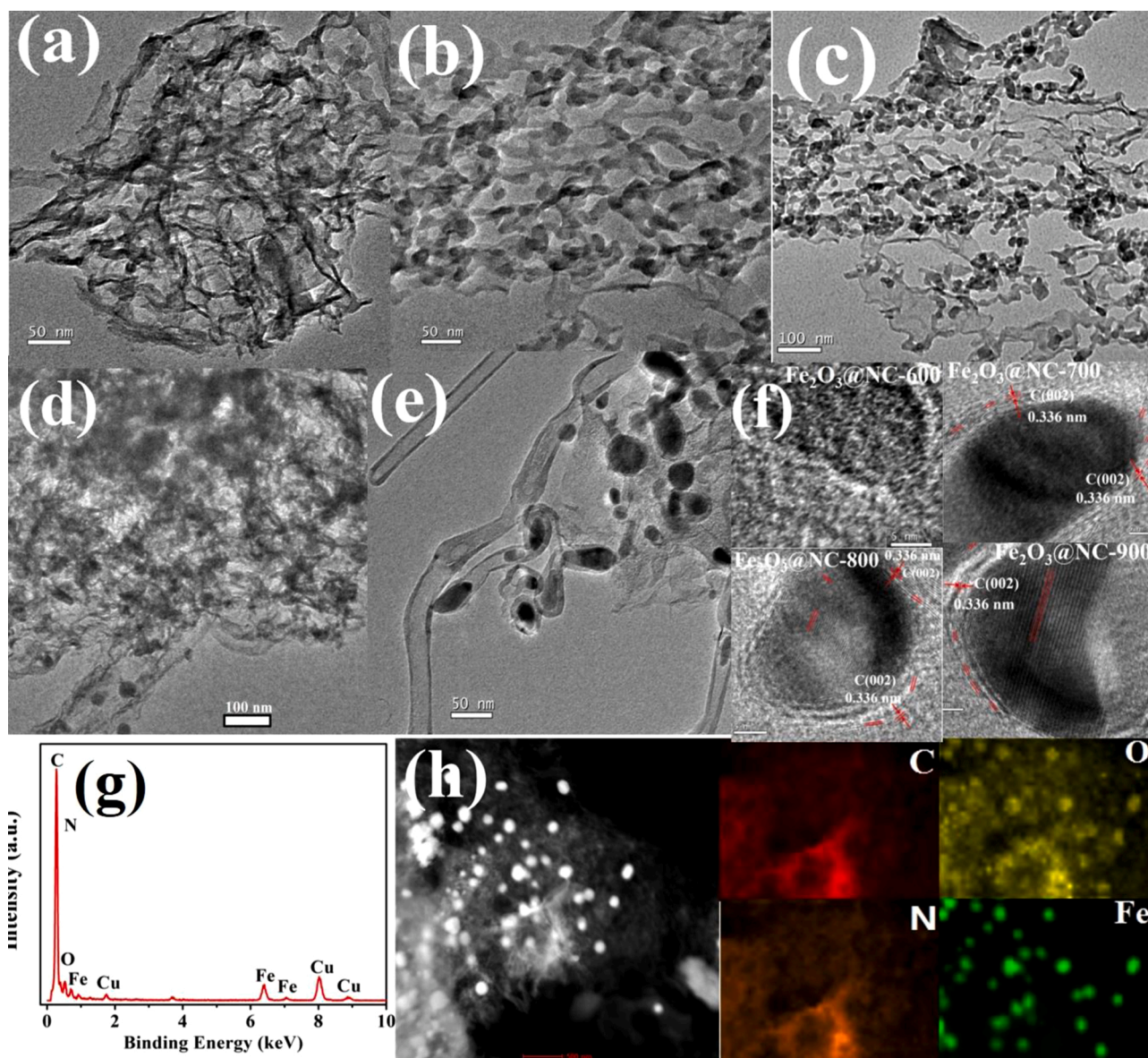

Fig. 1. Electron microscopy analysis of Fe$_2$O$_3$@NC catalysts: TEM images of (a) Fe$_2$O$_3$@NC-500, (b) Fe$_2$O$_3$@NC-600, (c) Fe$_2$O$_3$@NC-700, (d) Fe$_2$O$_3$@NC-800, (e) Fe$_2$O$_3$@NC-900; (f) HRTEM images of Fe$_2$O$_3$@NC-600, Fe$_2$O$_3$@NC-700, Fe$_2$O$_3$@NC-800 and Fe$_2$O$_3$@NC-900; (g) EDX analysis of Fe$_2$O$_3$@NC-800; (h) element distribution diagram of Fe$_2$O$_3$@NC-800.
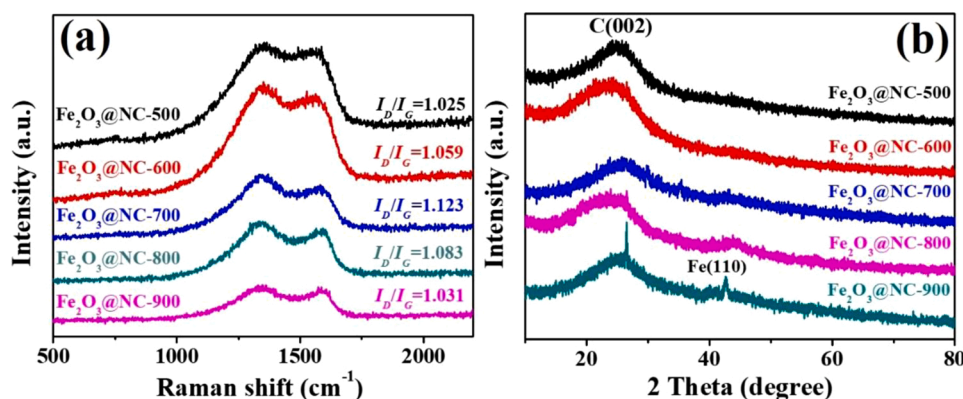
Fig. 2. (a) Raman spectra and (b) XRD patterns of a series of Fe_2O_3@NC catalysts.

Hence, a weight loss of 44.1 % is observed between 144 °C and 245 °C. When the temperature reached 356 °C, the weight of the precursor material decreased by 28.0 %, probably due to the pyrolysis of a majority of the oxygen-containing functional groups in the precursor. At a temperature greater than 356 °C, pyrolysis was almost completed, and the material weight slowly decreased.

TEM analysis revealed that the calcination temperature obviously affects the morphology of the prepared catalyst (Fig. 1a-e). When calcinated at 500 °C, Fe_2O_3@NC-500 exhibited a pleated nanosheet, which makes it difficult to observe Fe_2O_3 NPs (Fig. 1a). This is probably related to the difficulty in transferring Fe^{3+} to Fe_2O_3 NPs at 500 °C and failure to form the related Fe_2O_3 NPs. TEM image of Fe_2O_3@NC-600 revealed that the morphology of the catalyst prepared at 600 °C remains unchanged, but the Fe_2O_3 NPs started to form (Fig. 1b). Fig. 1c shows TEM image of Fe_2O_3@NC-700. The average particle size of Fe_2O_3 NPs in Fe_2O_3@NC-700 is about 12 nm. However, the morphology of the carbon matrix was changed. With increase in the carbonization temperature to 800 °C, the Fe_2O_3 NPs still maintained a smaller size with an average diameter of

approximately 15 nm (Fig. 1d). N-doped carbon carriers were continuously pyrolyzed and transferred toward carbon nanotubes. Fe_2O_3@NC-800 is a type of a floccule porous material between the folded nanosheet and nanotube. The TEM image of Fe_2O_3@NC-900 revealed that the N-doped carbon carrier changes to nanotubes and that Fe_2O_3 NPs with an average diameter of 20 nm are wrapped within the nanotube (Fig. 1e). Therefore, the calcination temperature affects the particle size of Fe_2O_3 NPs in the Fe_2O_3@NC catalysts and the morphology of N-doped carbon materials. High calcination temperatures afford large Fe_2O_3 NPs, and because Fe is one of the catalysts used to prepare carbon nanotubes, the carbon matrix in the material is gradually converted into carbon nanotubes [33]. HRTEM images of Fe_2O_3@NC-600, Fe_2O_3@NC-700, Fe_2O_3@NC-800, and Fe_2O_3@NC-900 revealed that Fe_2O_3 NPs are coated with N-doped carbon (Fig. 1f). The lattice fringe of the C(002) crystal surface wrapped around Fe_2O_3 NPs is observed. The EDX analysis of Fe_2O_3@NC-800 confirmed the presence of Fe, C, N, and O in Fe_2O_3@NC-800 (Fig. 1g). The elemental distribution of Fe_2O_3@NC-800 confirmed the successful embedding of Fe_2O_3 NPs into N-doped carbon
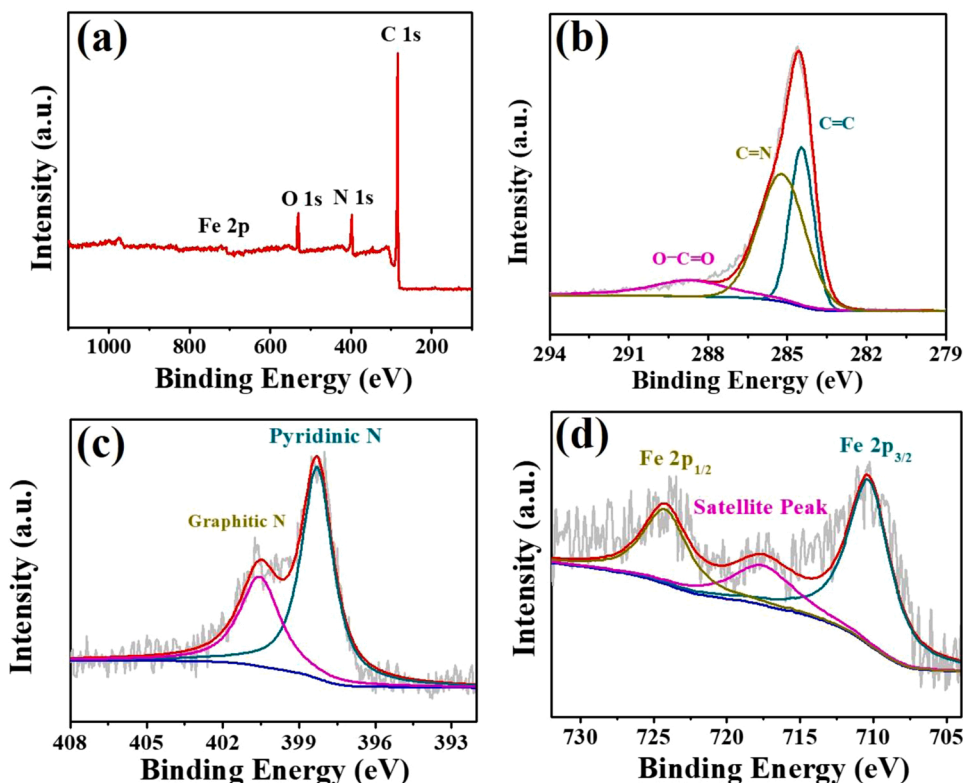

Fig. 3. XPS analysis of Fe_2O_3@NC-800 (a),C 1s (b), N 1s (C) and Fe 2p (d).

(Fig. 1h).

Raman spectra mainly showed that D (1350 cm^{-1}) and G (1587 cm^{-1}) peaks for a series of Fe$_2$O$_3$@NC catalysts varied with the temperature (Fig. 2a). The relative intensity ratio of I$_D$/I$_G$ represents the density of defects in the catalysts. The I$_D$/I$_G$ value exerted a certain relationship with the carbonization temperature. The I$_D$/I$_G$ firstly increased and then decreased. Moreover, with increase in carbonization temperature to 700 °C, the I$_D$/I$_G$ value was the maximum, and then it decreased with increased carbonization temperature. The higher the carbonization temperature, the higher the graphitization degree of the prepared materials. However, due to the effect of Fe, additional defects were observed in the vicinity of Fe$_2$O$_3$ NPs. Therefore, this change is caused by the effect of changes from carbon matrix to carbon nanotubes with increase in carbonization temperature. XRD patterns of different Fe$_2$O$_3$@NC materials shows a wide diffraction peak at 26°, corresponding to the presence of the C(002) crystal plane in all samples (Fig. 2b). Especially, Fe$_2$O$_3$@NC-900 prepared at a high carbonization temperature of 900 °C exhibited strong peak strength. By comparing the XRD patterns of different Fe$_2$O$_3$@NC samples, a new peak at 44.7° which attributed to Fe(110) crystal plane was observed in Fe$_2$O$_3$@NC-900 pattern [34]. In addition, it was difficult to observe the characteristic peak for the Fe(110) crystal plane in Fe$_2$O$_3$@NC-500, Fe$_2$O$_3$@NC-600, Fe$_2$O$_3$@NC-700, and Fe$_2$O$_3$@NC-800, because Fe NPs were hardly formed at such carbonization temperatures.

To investigate the specific surface area, pore diameter and pore volume of Fe$_2$O$_3$@NC-800, nitrogen adsorption–desorption isotherms were recorded (Fig. S2a). A typical type IV nitrogen adsorption isotherm was observed for Fe$_2$O$_3$@NC-800, and hysteresis was observed in the region of the medium and high pressures, near P/P$_0$ = 0.4, the relative pressure of closed, indicative of a mainly mesoporous aperture distribution for Fe$_2$O$_3$@NC-800 [35]. The specific surface area of Fe$_2$O$_3$@NC-800 was 418.8 m^2 g^{-1}. Such a high specific surface area plays an active role in catalysis. Fig. S2b shows the aperture distribution curve of Fe$_2$O$_3$@NC-800. Consistent with the conclusion from the nitrogen adsorption–desorption isotherm analysis, the types of pores in Fe$_2$O$_3$@NC-800 are mainly mesoporous: at 4.2 nm and 20–50 nm. Mesopores are more favorable for the diffusion of the substrate within an abundant pore size distribution.

Fig. 3a shows the wide-spectrum XPS of Fe$_2$O$_3$@NC-800 catalyst. The result was consistent with the EDX results: C, N, O, and Fe were present in Fe$_2$O$_3$@NC-800. The characteristic signal of Fe 2p was relatively weak, possibly caused by Fe$_2$O$_3$ NPs being surrounded by N-doped carbon. Fig. 3b shows the high-resolution C 1s spectrum of Fe$_2$O$_3$@NC-800. The C in Fe$_2$O$_3$@NC-800 mainly existed as C=C (284.6 eV) and CN= (285.3 eV). The characteristic signal for O—CO= in the sample was observed at 288.7 eV with weak strength, confirming that the considerable pyrolysis of oxygen-containing functional groups occurs in the catalyst during carbonization. Fig. 3c shows the high-resolution N 1s spectrum of Fe$_2$O$_3$@NC-800. The two peaks at 398.1 and 400.7 eV corresponded to pyridine N and graphite N, respectively [36]. Through XPS analysis, the N content of Fe$_2$O$_3$@NC-800 was 12. 28 %, and the corresponding contents of pyridine N and graphite N were 7.98 % and 4.3 %, respectively. Fig. 3d shows the high-resolution Fe 2p spectrum of Fe$_2$O$_3$@NC-800. The Fe 2p$_{3/2}$ signal with a combined energy of 710.7 eV and the Fe 2p$_{1/2}$ signal with a combined energy of 723.0 eV were observed in the spectrum, indicating that Fe element is existing as Fe$_2$O$_3$ in Fe$_2$O$_3$@NC-800 sample [37,38]. It is worth mentioning that the satellite peak around 719.0 eV also suggests that the iron oxide is the main Fe species in Fe$_2$O$_3$@NC-800 sample [39]. In addition, Fe-N$_x$ was not observed in Fe@NC-800 (whose characteristic signal was observed at 713.4 eV), providing supplementary evidence for the active component in the catalytic reaction. **Table S1** summarizes the contents of N and Fe in Fe$_2$O$_3$@NC-800. As determined by elemental analysis, the contents of N in Fe$_2$O$_3$@NC-500, Fe$_2$O$_3$@NC-600, Fe$_2$O$_3$@NC-700, Fe$_2$O$_3$@NC-800, and Fe$_2$O$_3$@NC-900 were 27.20 %, 25.15 %, 15.12 %, 14.06 %, and 7.14 %, respectively, and the corresponding Fe contents estimated by

Table 1

Preparation of benzonitrile from benzaldehyde and ammonia by catalysts: comparison of catalytic activity under different conditions.[a]

	Catalyst	T (°C)	Ammonia (μL)	Solvent	Yield (%)
1	Fe$_2$O$_3$@NC-500 (30 mg)	60	800	EtOH	0.15
2	Fe$_2$O$_3$@NC-600 (30 mg)	60	800	EtOH	0.42
3	Fe$_2$O$_3$@NC-700 (30 mg)	60	800	EtOH	32.00
4	Fe$_2$O$_3$@NC-800 (30 mg)	60	800	EtOH	69.25
5	Fe$_2$O$_3$@NC-900 (30 mg)	60	800	EtOH	59.79
6	NCNS (50 mg)	60	800	EtOH	trace
7	Fe$_2$O$_3$@NC-800 (10 mg)	60	800	EtOH	13.26
8	Fe$_2$O$_3$@NC-800 (50 mg)	60	800	EtOH	99.45
9	Fe$_2$O$_3$@NC-800 (50 mg)	60	800	DMSO	78.61
10	Fe$_2$O$_3$@NC-800 (50 mg)	60	800	DMF	49.37
11	Fe$_2$O$_3$@NC-800 (50 mg)	60	800	1, 2-Dichloroethane	29.93
12	Fe$_2$O$_3$@NC-800 (50 mg)	60	800	*n*-Hexane	27.25
13	Fe$_2$O$_3$@NC-800 (50 mg)	50	800	EtOH	96.39
14	Fe$_2$O$_3$@NC-800 (50 mg)	70	800	EtOH	69.65
15	Fe$_2$O$_3$@NC-800 (50 mg)	60	600	EtOH	46.82
16	Fe$_2$O$_3$@NC-800 (50 mg)	60	700	EtOH	63.64

[a] Reaction condition: benzaldehyde (1 mmol), solvent (5 mL), ammonia (28 %–30 %) and at O$_2$ atmosphere for 24 h.
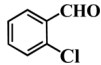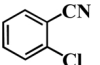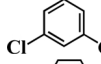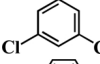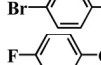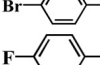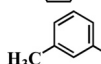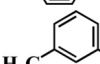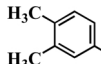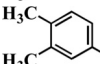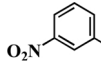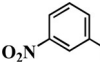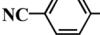
ICP–OES were 1.73 %, 1.88 %, 4.22 %, 5.43 %, and 6.03 %.

2.2. Catalytic ammoxidation of benzaldehyde to benzonitrile

The catalytic properties of the prepared Fe$_2$O$_3$@NC materials were examined by ammoxidation of benzaldehyde to benzonitrile. Table 1 summarizes the optimization of reaction conditions. Fe$_2$O$_3$@NC catalysts prepared at different calcination temperatures exhibited different catalytic properties under the same reaction conditions, and Fe$_2$O$_3$@NC-800 exhibited the highest catalytic activity (entries 1–5). When N-doped carbon nanosheets (NCNS) without iron was used as the catalyst, there was no conversion of benzaldehyde (entry 6), indicating that the Fe$_2$O$_3$ should be the active sites for the catalytic ammoxidation of benzaldehyde to benzonitrile. With the reduction in the amount of the Fe$_2$O$_3$@NC-800 catalyst to 10 mg, the conversion rate of benzaldehyde was low at 24 h (entry 7). By using 50 mg of the Fe$_2$O$_3$@NC-800 catalyst, almost all of the benzaldehyde was converted into benzonitrile at 24 h (entry 8). Low-polarity solvents gave poor reaction results, and the yield of benzonitrile accordingly decreased with the gradual decrease in the solvent polarity (entries 8–12). Therefore, ethanol is the optimal solvent herein. Reaction temperature certainly affected the reaction yield. The yield of benzonitrile was the highest at 60 °C, and the yield decreased with the decrease in the temperature to 50 °C (entry 13). However, with increase in reaction temperature to 70 °C, the benzonitrile yield reduces to about 70 %. The reason is that, in a high reaction temperature of above 70 °C, the volatilization of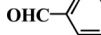 NH$_3$ from the reaction mixture will lead the reduction of the NH$_3$H$_2$O concentration, which is not conducive to the ammoxidation reaction. The ammonia content of ammonia water led to the significant reduction in the yield of benzonitrile due to

Table 2

Fe$_2$O$_3$@NC-800 catalyzed ammoxidation of aromatic aldehydes to benzonitriles.[a]

Entry	Substrate	Product	Conv. (%)	Sel. (%)
1	2-Cl-C$_6$H$_4$-CHO	2-Cl-C$_6$H$_4$-CN	62.92	>99
2	3-Cl-C$_6$H$_4$-CHO	3-Cl-C$_6$H$_4$-CN	63.78	>99
3	4-Br-C$_6$H$_4$-CHO	4-Br-C$_6$H$_4$-CN	78.72	>99
4	4-F-C$_6$H$_4$-CHO	4-F-C$_6$H$_4$-CN	86.49	>99
5	3-CH$_3$-C$_6$H$_4$-CHO	3-CH$_3$-C$_6$H$_4$-CN	89.97	>99
6	3,4-(CH$_3$)$_2$-C$_6$H$_3$-CHO	3,4-(CH$_3$)$_2$-C$_6$H$_3$-CN	92.41	>99
7	3-O$_2$N-C$_6$H$_4$-CHO	3-O$_2$N-C$_6$H$_4$-CN	49.38	>99
8	OHC-C$_6$H$_4$-CHO	NC-C$_6$H$_4$-CN	80.70	>99

[a] Reaction condition: substrate (1 mmol), EtOH (5 mL), 800 μL ammonia (28 %–30 %), catalyst (50 mg) and under O$_2$ atmosphere for 24 h at 60 ℃.
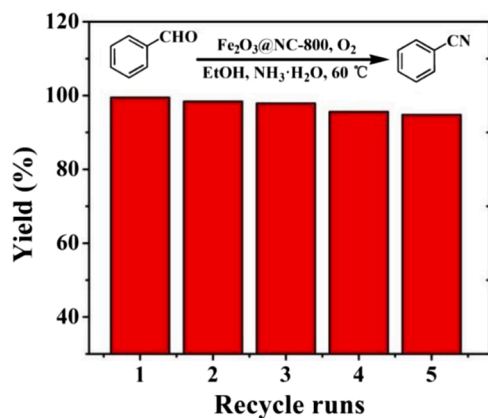

Fig. 4. Recyclability of Fe$_2$O$_3$@NC-800 for catalytic ammonia oxidation of benzaldehyde.

ammonia evaporation (entry 14). This study also examined the effect of the amount of ammonia on the reaction yield, and the decrease in the amount of ammonia led to the decrease in the yield of benzonitrile (entries 15–16). The Scheme in Table 2 shows the possible reaction mechanism for the formation of benzonitrile from benzaldehyde. Imine intermediates were formed from aldehyde and ammonia. The elimination of a H$_2$ molecule from this produced intermediate finally afforded the corresponding nitriles in the presence of the Fe$_2$O$_3$@NC-800 catalyst [24].

In addition, Fe$_2$O$_3$@NC-800 was used to prepare nitrile by the ammoxidation of other aromatic aldehydes under optimal reaction conditions (Table 2). For various halogen-substituted benzaldehydes, good conversion and eminent selectivity at 24 h were observed (entries 1–4). The results revealed that the aromatic aldehydes substituted by different halogens are affected by the halogen species. When the substituent is changed to an electron-donating methyl group, a high substrate conversion was observed (entry 5). With the increase in the number of methyl groups, the substrate conversion increased to 92.41 % while still maintaining excellent selectivity (entry 6). However, when the substituent is a nitro group, with a higher electron withdrawing

capacity, the yield of aromatic aldehydes significantly decreased. Under the same reaction conditions, only 49.38 % of *m*-nitrobenzaldehyde was converted into *m*-nitrobenzonitrile (entry 7). With the increase in the number of aldehyde groups, the reaction still maintained good conversion and excellent selectivity. Without the increase in the amount of ammonia, the yield of *p*-diphenylnitrile reached 80.70 % at 24 h (entry 8). Thus, the Fe$_2$O$_3$@NC-800 exhibits good general applicability for ammoxidation of aromatic aldehydes to nitriles.

The reusability of Fe$_2$O$_3$@NC-800 was investigated by the catalytic ammoxidation of benzaldehyde to benzonitrile. All of the catalytic cycle experiments were completed within 24 h, and the yield of benzonitrile was maintained to be greater than 95 % (Fig. 4). There is no Fe element was detected in the reaction solution after the catalytic ammoxidation reaction using ICP-OES measurement. The TEM image of the recycled Fe$_2$O$_3$@NC-800 also showed that, the morphology of the spent Fe$_2$O$_3$@NC-800 catalyst was almost the same as the fresh Fe$_2$O$_3$@NC-800 catalyst (Fig. S3). These repeated experiments confirmed that as-prepared Fe$_2$O$_3$@NC-800 catalyst exhibits good chemical stability and recyclability in the catalytic ammoxidation of benzaldehyde.

3. Conclusion

In this study, an N-doped carbon-coated iron oxide nanoparticles catalyst (Fe$_2$O$_3$@NC-800) was successfully prepared using renewable biomass chitosan, cost-effective urea, and abundant ferric chloride as precursors. Iron oxide NPs uniformly and considerably dispersed in the Fe$_2$O$_3$@NC-800 catalyst and wrapped within N-doped carbon. Fe$_2$O$_3$@NC-800 exhibited prominentcatalytic activity and selectivity for the ammoxidation of aromatic aldehydes. This study provides a cost-effective, simple strategy for the synthesis of non-noble-metal-modified N-doped carbon catalysts for the ammoxidation of aldehydes.

Declaration of Competing Interest

There are no conflicts of interest to declare.

Acknowledgements

Appendix A. Supplementary data

Supplementary material related to this article can be found, in the online version, at doi:https://doi.org/10.1016/j.mcat.2020.111293.

References

[1] I.Y. Jeon, H.J. Noh, J.B. Baek, Nitrogen-doped carbon nanomaterials: synthesis, characteristics and applications, Chem. Asian J. 15 (2020) 2282–2293.

[2] Z.S. Shi, W.Q. Yang, Y.T. Gu, T. Liao, Z.Q. Sun, Metal-nitrogen-doped carbon materials as highly efficient catalysts: progress and rational design, Adv. Sci. 7 (2020), 2001069.

[3] P. Sun, H. Liu, M.B. Feng, L. Guo, Z.C. Zhai, Y.S. Fang, X.S. Zhang, V.K. Sharma, Nitrogen-sulfur co-doped industrial graphene as an efficient peroxymonosulfate activator: singlet oxygen-dominated catalytic degradation of organic contaminants, Appl. Catal. B: Environ. 251 (2019) 335–345.

[4] H.Y. Zhou, J.C. Li, Z. Wen, Q. Jiang, Tuning the catalytic activity of a single Mo atom supported on graphene for nitrogen reduction via Se atom doping, Phys. Chem. Chem. Phys. 21 (2019) 14583–14588.

[5] Q.P. Ke, Y.X. Jin, F. Ruan, M.N. Ha, D.D. Li, P.X. Cui, Y.L. Cao, H. Wang, T.T. Wang, V.N. Nguyen, X.Y. Han, X. Wang, P. Cui, Boosting the activity of catalytic oxidation of 5-hydroxymethylfurfural to 2,5-diformylfuran over nitrogen-doped manganese oxide catalysts, Green Chem. 21 (2019), 3701-3701.

[6] C. Falco, M. Sevilla, R.J. White, R. Rothe, M.M. Titirici, Renewable nitrogen-doped hydrothermal carbons derived from microalgae, Chemsuschem 5 (2012) 1834–1840.

[7] Jiangyong Liu, Jinxing Li, Rongfei Ye, Xiaodong Yan, Lixia Wang, Panming Jian, Versatile bifunctional nitrogen-doped porous carbon derived from biomass in catalytic reduction of 4-nitrophenol and oxidation of styrene, Chinese J. Catal. 41 (2020) 1217–1229.

[8] Chao Wang, Hanwei Wang, Baokang Dang, Zhe Wang, Xiaoping Shen, Caicai Li, Qingfeng Sun, Ultrahigh yield of nitrogen doped porous carbon from biomass waste for supercapacitor, Renew. Energy 156 (2020) 370–376.

[9] J.R. Yang, F. Shen, M. Qiu, X.H. Qi, Nitrogen-doped porous carbon derived from chitosan for the enhanced dehydrochlorination of lindane under mild conditions, Environ. Sci. Pollut. R 25 (2018) 35646–35656.

[10] Xiao Chen, Wen-Da Oh, Peng-Hui Zhang, Richard D. Webster, Teik-Thye Lim, Surface construction of nitrogen-doped chitosan-derived carbon nanosheets with hierarchically porous structure for enhanced sulfacetamide degradation via peroxymonosulfate activation: maneuverable porosity and active sites, Chem. Eng. J. 382 (2020), 122908.

[11] Yongjun Gao, Xi Chen, Jiaguang Zhang, Ning Yan, Chitin-Derived Mesoporous, Nitrogen-containing carbon for heavy-metal removal and styrene epoxidation, ChemPlusChem 80 (2015) 1556–1564.

[12] Yifan Shen, Yu Zhou, Lili Jiang, Guangni Ding, Luo. Luo, Zhaoguo Zhang, Xiaomin Xie, Selective aerobic oxidation of benzylic amines to aryl nitriles catalyzed by CuBr₂/N-methyl imidazole, Tetrahedron 74 (2018) 4266–4271.

[13] Hiroyuki Okabe, Asuka Naraoka, Takahiro Isogawa, Shunsuke Oishi, Hiroshi Naka, Acceptor-controlled transfer dehydration of amides to nitriles, Org. Lett. 21 (2019) 4767–4770.

[14] Yunzhu Wang, Shinya Furukawa, Zhang. Zhang, Laura Torrente-Murciano, Saif A. Khan, Ning Yan, Oxidant free conversion of alcohols to nitriles over Ni-based catalysts, Catal. Sci. Technol. 9 (2019) 86–96.

[15] Kengo Hyodo, Saki Kitagawa, Masayuki Yamazaki, Kingo Uchida, Iron-catalyzed dehydration of aldoximes to nitriles requiring neither other reagents nor nitrile media, Chem. Asian J. 11 (2016) 1348–1352.

[16] Eng-Chi Wang, Gow-Juin Lin, A new one pot method for the conversion of aldehydes into nitriles using hydroxyamine and phthalic anhydride, Tetrahedron Lett. 39 (1998) 4047–4050.

[17] B.V. Rokade, K.R. Prabhu, Chemoselective schmidt reaction mediated by triflic acid: selective synthesis of nitriles from aldehydes, J. Org. Chem. 77 (2012) 5364–5370.

[18] Chaojie Fang, Meichao Li, Xinquan Hu, Weimin Mo, Baoxiang Hu, Nan Sun, Liqun Jin, Zhenlu Shen, A practical iodine-catalyzed oxidative conversion of aldehydes to nitriles, RSC Adv. 7 (2017) 1484–1489.

[19] Jitendra Gurjar, Jorick Bater, Valery Fokin, Sulfuryl fluoride mediated conversion of aldehydes to nitriles, Chem. - A Eur. J. 25 (2018) 1906–1909.

[20] Antonella Leggio, Emilia Lucia Belsito, Sonia Gallo, Angelo Liguori, One-pot conversion of aldehydes to nitriles mediated by TiCl₄, Tetrahedron Lett. 58 (2017) 1512–1514.

[21] T. Kropp, M. Mavrikakis, Transition metal atoms embedded in graphene: how nitrogen doping increases CO oxidation activity, ACS Catal. 9 (2019) 6864–6868.

[22] B. Li, Y. Chen, X.M. Ge, J.W. Chai, X. Zhang, T.S.A. Hor, G.J. Du, Z.L. Liu, H. Zhang, Y. Zong, Mussel-inspired one-pot synthesis of transition metal and nitrogen co-doped carbon (M/N-C) as efficient oxygen catalysts for Zn-air batteries, Nanoscale 8 (2016) 5067–5075.

[23] Yueling Cao, Bowen Zhao, Xiaobing Bao, Yong Wang, Fabricating Metal@N-Doped carbon catalysts via a thermal method, ACS Catal. 8 (2018) 7077–7085.

[24] Yunzhu Wang, Shinya Furukawa, Ning Yan, Identification of an active NiCu catalyst for nitrile synthesis from alcohol, ACS Catal. 9 (2019) 6681–6691.

[25] Yunzhu Wang, Shinya Furukawa, Xinpu Fu, Ning Yan, Organonitrogen chemicals from oxygen-containing feedstock over heterogeneous catalysts, ACS Catal. 10 (2020) 311–335.

[26] J.C. Li, M. Cheng, T. Li, L. Ma, X.F. Ruan, D. Liu, H.M. Cheng, C. Liu, D. Du, Z. D. Wei, Y. Lin, M. Shao, Carbon nanotube-linked hollow carbon nanospheres doped with iron and nitrogen as single-atom catalysts for the oxygen reduction reaction in acidic solutions, J. Mater. Chem. A Mater. Energy Sustain. 7 (2019) 14478–14482.

[27] J.Q. Tuo, Y.H. Zhu, L. Cheng, Y.H. Li, X.L. Yang, J.H. Shen, C.Z. Li, Layered Confinement Reaction: Atomic-level Dispersed Iron-Nitrogen Co-Doped Ultrathin Carbon Nanosheets for CO₂ Electroreduction, Chemsuschem 12 (2019) 2644–2650.

[28] C.B. Lu, J.C. Zhang, Z.Y. Chen, K.Y. Jiang, M.Q. Li, F. Zhang, G.S. Tong, X.X. Zou, Y.Z. Su, X.D. Zhuang, A room-temperature interfacial approach towards iron/ nitrogen co-doped fibrous porous carbons as electrocatalysts for the oxygen reduction reaction and Zn-Air batteries, Nanoscale 11 (2019) 10257–10265.

[29] H.B. Tan, J. Tang, J. Kim, Y.V. Kaneti, Y.M. Kang, Y. Sugahara, Y. Yamauchi, Rational design and construction of nanoporous iron- and nitrogen-doped carbon electrocatalysts for oxygen reduction reaction, J. Mater. Chem. A 7 (2019) 1380–1393.

[30] K. Wang, H.X. Chen, X.F. Zhang, Y.X. Tong, S.Q. Song, P. Tsiakaras, Y. Wang, Iron oxide@graphitic carbon core-shell nanoparticles embedded in ordered mesoporous N-doped carbon matrix as an efficient cathode catalyst for PEMFC, Appl. Catal. B: Environ. 264 (2020), 118468.

[31] Ran Hao, Jin-Tao Ren, Xian-Wei Lv, Wei Li, Yu-Ping Liu, Zhong-Yong Yuan, N - doped porous carbon hollow microspheres encapsulated with iron -based nanocomposites as advanced bifunctional catalysts for rechargeable Zn-air battery, J. Energy Chem. 49 (2020) 14–21.

[32] H. Meng, S. Gao, M.M. Luo, X.M. Zeng, Iron and phenol Co-catalysis for rapid synthesis of nitriles under mild conditions, Eur. J. Org. Chem. (2019) 4617–4623.

[33] Manoj Pudukudy, Zahira Yaakob, Khaleeda Mhd Syahri, Qingming Jia, Shaoyun Shan, Production of hydrogen-rich syngas and multiwalled carbon nanotubes by biogas decomposition over zirconia supported iron catalysts, J. Ind. Eng. Chem. 84 (2020) 150–166.

[34] Zhuo Zong, Zhengxin Qian, Zhenghua Tang, Zhen Liu, Yong Tian, Shaohua Wang, Hydrogen evolution and oxygen reduction reactions catalyzed by core-shelled Fe@ Ru nanoparticles embedded in porous dodecahedron carbon, J. Alloys. Compd. 784 (2019) 447–455.

[35] Guang Gao, Peng Sun, Yunqin Li, Fang Wang, Zelun Zhao, Yong Qin, Fuwei Li, Highly stable porous-carbon-Coated Ni catalysts for the reductive amination of levulinic acid via an unconventional pathway, ACS Catal. 7 (2017) 4927–4935.

[36] Yang. Yang, Zhengyan Lun, Guoliang Xia, Fangcai Zheng, Mengni He, Qianwang Chen, Non-precious alloy encapsulated in nitrogen-doped graphene layers derived from MOFs as an active and durable hydrogen evolution reaction catalyst, Energy Environ. Sci. 8 (2015) 3563–3571.

[37] Chunsen Song, Shikui Wu, Xiaoping Shen, Xuli Miao, Zhenyuan Ji, Aihua Yuan, Keqiang Xu, Miaomiao Liu, Xulan Xie, Lirong Kong, Guoxing Zhu, Sayyar Ali Shah, Metal-organic framework derived Fe/Fe₃C@N-doped-carbon porous hierarchical polyhedrons as bifunctional electrocatalysts for hydrogen evolution and oxygen-reduction reactions, J. Colloid Interf. Sci. 524 (2018) 93–101.

[38] A.P. Grosvenor, B.A. Kobe, M.C. Biesinger, N.S. McIntyre, Investigation of multiplet splitting of Fe 2p XPS spectra and bonding in iron compounds, Surf. Interface Anal. 36 (2004) 1564–1574.

[39] M. Tian, X.L. Cui, K. Liang, J.T. Ma, Z.P. Dong, Efficient and chemoselective hydrogenation of nitroarenes by gamma-Fe₂O₃ modified hollow mesoporous carbon microspheres, Inorg. Chem. Front. 3 (2016) 1332–1340.